Testing High-Energy Emission Models for Blazars with X-ray Polarimetry

Abel L. Peirson [ID],[1] Ioannis Liodakis [ID],[2] and Roger W. Romani [ID][1]

[1]*Kavli Insitute for Particle Astrophysics and Cosmology, Stanford University, Stanford, CA 94305, USA*
[2]*Finnish Centre for Astronomy with ESO, University of Turku, Vesilinnantie 5, FI-20014, Finland*

ABSTRACT

Both leptonic and hadronic emission processes may contribute to blazar jet emission; which dominates in blazars's high energy emission component remains an open question. Some intermediate synchrotron peaked blazars transition from their low to high energy emission components in the X-ray band making them excellent laboratories to probe both components simultaneously, and good targets for the newly launched Imaging X-ray Polarimetry Explorer. We characterize the spectral energy distributions for three such blazars: CGRaBS J0211+1051, TXS 0506+056, and S5 0716+714, predicting their X-ray polarization behavior by fitting a multizone polarized leptonic jet model. We find that a significant detection of electron synchrotron dominated polarization is possible with a 300 ks observation for S5 0716+714 and CGRaBS J0211+1051 in their flaring states, while even 500 ks observations are unlikely to measure synchrotron self-Compton polarization. Importantly, non-leptonic emission processes like proton synchrotron are marginally detectable for our brightest ISP, S5 0716+714, during a flaring state. Improved *IXPE* data reduction methods or next generation telescopes like *eXTP* are needed to confidently measure SSC polarization.

Keywords: Polarization — X-rays: galaxies — X-rays: general — Galaxies: jets

1. INTRODUCTION

Blazars are active galactic nuclei whose relativistic jets are oriented at an angle $\theta_{\rm obs}$ within a few degrees, typically $< 15^o$ (Liodakis et al. 2018), from an observer on Earth. This results in the relativistically boosted emission from the jet to outshine the host galaxy. The jet's observed multiwavelength emission, from radio to γ-rays, is characterized by two broad components. The low-energy component is attributed to synchrotron emission from primary jet electrons, while the high-energy component is still unknown with inverse-Compton (IC) scattering or hadronic processes (proton synchrotron, pion cascades, etc.) as the current favored mechanisms (Blandford et al. 2019). Blazars are often classified by the peak frequency (ν_{Sy}) of the low-energy component (Abdo et al. 2010). Here we focus on the "Intermediate Synchrotron Peak" (ISP) blazars, whose synchrotron emission peaks in optical/UV and have their spectral energy distributions (SEDs) dropping toward eventual high-energy component dominance in the hard

alpv95@stanford.edu

X-ray/γ-ray band. In particular, we focus on a subclass of ISPs whose X-ray emission lies in the valley formed by the combination of the two spectral components.

While the origin of the high-energy component is still unknown, the recent launch of the Imaging X-ray Polarimetry Explorer (*IXPE*, Weisskopf et al. 2021) offers a new diagnostic tool to probe the jet physics, composition, and acceleration of particles. In Liodakis et al. (2019) we used a multizone jet model (Marscher 2014; Peirson & Romani 2018, 2019) and optical polarization results from the RoboPol survey (Blinov et al. 2021) to make predictions for the X-ray polarization degree of blazars. In a synchrotron self-Compton (SSC) scenario, we expect substantial polarization from the electron synchrotron and much lower polarization levels from the Compton component. On the other hand, the polarization degree of proton-synchrotron and synchrotron from hadron initiated pair cascades is expected to be much higher than that of IC emission and comparable to that of the primary electron synchrotron component. Interestingly, as one observes further out on the electron synchrotron cut-off tail, fewer jet emission zones have sufficient particle energies and Doppler factors to produce the detected radiation – this means that there is de-

creased polarization angle (PA) averaging between emission zones and thus larger net synchrotron polarization degree and higher variability (Peirson & Romani 2018, 2019). Polarization measurements in the transition region between low- and high-energy components can thus be a powerful tool to probe not only for the high-energy emission processes, but also the jet and magnetic field structure. Coincidentally, recent hybrid (also known as lepto-hadronic) blazar models for the high-energy neutrino emission suggest the existence of subdominant synchrotron components from proton initiated pair cascades that might only be detectable in the transition valley where any primary lepton emission is minimized (e.g., Gao et al. 2019). All of the above suggest that ISPs, whose transition regions lie in the 1-10 keV band are particularly attractive targets for current and future X-ray polarization missions.

We have identified three such sources, namely CGRaBS J0211+1051, TXS 0506+056, and S5 0716+714. CGRaBS J0211+1051 and S5 0716+714 are first year *IXPE* targets, while CGRaBS J0211+1051 and TXS 0506+056 are potential neutrino emitters (Ice-Cube Collaboration et al. 2018; Hovatta et al. 2021). Our goal is twofold: (1) understand the polarization behaviour of the jet across the transition region; (2) make predictions for *IXPE* and future missions to understand the high-energy emission signatures from blazars. In section 2 we describe the data and jet models, in section 3 we make predictions for *IXPE*, and in section 4 we discuss our findings.

2. MULTIWAVELENGTH OBSERVATIONS AND MODELING

The non-X-ray multiwavelength data for all sources are taken from the Space Science data center archive[1]. The data are not contemporaneous and include both flaring and quiescent periods of each source. Since the latter may allow improved polarization measurements, we analyze quiescent and flaring data separately. We bin the observations in frequency bins of 0.1 dex and treat the resulting SED as an "average" SED of the source in the given state. Examples are shown in Fig. 1.

For the X-ray observations we used publicly available Neil Gehrels Swift Observatory (*Swift*), *NuSTAR* and XMM-Newton data from the High Energy Astrophysics Science Archive Research Center (HEASARC) browse interface. The X-ray observations for the source in normal and flaring (f) states are drawn from the following date ranges: CGRaBS J0211+1051(f) (MJD

---
[1] https://tools.ssdc.asi.it/SED/

55260-55886), CGRaBS J0211+1051 (MJD 59250), S5 0716+714(f) (MJD 57046), S5 0716+714 (MJD 54864-55920), TXS 0506+056(f) (MJD 58025). For CGRaBS J0211+1051 in quiescence we augment with a new $\sim$ 65 ks XMM-Newton observation (AO-19, ID number: 0861840101, MJD 59250). All *Swift* data used were contemporaneous (within 1-2 days) of exposures from one of the other facilities. The data were processed using the standard HEASARC tools and recommended analyses.

Previous fits to these data have typically used absorbed broken powerlaw models for TXS 0506+056 (IceCube Collaboration et al. 2018) and S5 0716+714 (Wierzcholska & Siejkowski 2016). Instead, we fit the extracted spectra, using *XSPEC*, with a more physically motivated model: the sum of two powerlaw components, subject to absorption by a Galactic neutral hydrogen column N_H. For CGRaBS J0211+1051, the publicly available *Swift* snapshots did not provide sufficient signal-to-noise to unambiguously determine the shape of the 1-10 keV spectrum. We thus tried three models, a single power-law, a power-law with an exponential cutoff, and a sum of two power-laws. We then used the Akaike information criterion to select the model that best describes the data. Again the sum of two power-laws is preferred. The best-fit model parameters are given in Table 1.

Table 1. X-ray spectral parameters

Name	N_H	Γ_2	Γ_1
CGRaBS J0211+1051	0.16	1.18±0.19	2.68±0.4
TXS 0506+056	0.25	1.83±0.2	3.88±1.0
S5 0716+714	0.031	1.56±0.33	2.36±0.14

NOTE—The N_H values are given in units of $\times 10^{22}\ cm^{-2}$.

2.1. *SED modeling*

Our joint SED and polarization modeling uses the polarized leptonic jet emission model developed in Peirson & Romani (2018, 2019), inspired partly by Potter & Cotter (2012); Marscher (2014). It assumes an initial power-law electron population propagating along a relativistic conical jet. The jet cross section is divided into multiple magnetic field zones, with isotropically distributed field orientations. These magnetic fields are comoving with the jet material. Polarized synchrotron emission is self-consistently calculated as the electron population

propagates and cools. SSC emission is computed, including the propagation of synchrotron photons from downstream emission into each Comptonizing zone. For quasi-spherical magnetic field zones, as often assumed in turbulent scenarios, the model resolves a decorrelation timescale (which depends on the initial jet parameters) of 0.5–5 days. This is the timescale over which steady state jet emission is expected to fluctuate.

An important feature of this jet model is variable Doppler boosting of the zones, since those directed closest to the line of sight increasingly dominant in the observed flux as the SED steepens (Peirson & Romani 2019). This guarantees an increasing expected polarization degree and larger polarization variability above the synchrotron peak. The X-ray SSC polarization degree is typically $\sim 0.2 - 0.35\times$ that of the synchrotron peak polarization; the components' PAs are highly correlated. In this model the observed synchrotron and SSC polarization behavior depends significantly on the geometric jet parameters, such as jet opening angle, observation angle, and Lorentz factor.

Our leptonic jet emission model is essentially independent of particle acceleration method since it follows zones downstream of any acceleration region. The assumed 'chaotic' disordered magnetic fields and relativistic boosting effects should be present in many magnetic reconnection and shock acceleration scenarios. We also assume steady-state emission, probing polarization variability by re-seeding the magnetic field zones. We briefly discuss how these simplifying assumptions may be violated in other models found in the literature in section 4.

In order to constrain our model's jet parameters, we fit the multiwavelength SED observations of each blazar state. Due to the chaotic magnetic field zones, our model is stochastic: the same jet parameters can result in different observed SEDs. A stochastic optimization method is necessary to fit such a model to fixed observations. We use a simple variant of the cross-entropy method (Rubinstein & Kroese 2004; Kochenderfer & Wheeler 2019). At each step, this samples n sets of jet parameters from a multivariate Gaussian and re-fits a new Gaussian using k samples with the lowest χ^2. Steps are repeated until convergence, when the mean and covariance matrix of the Gaussian no longer change significantly between steps. We use $n = 80, k = 20$. Since the multiwavelength SEDs for each blazar are not simultaneous and the true SEDs can be much more variable than the observational errors imply, we make the simplifying assumption that every observation has the same error. Our jet model has 8 free parameters. We
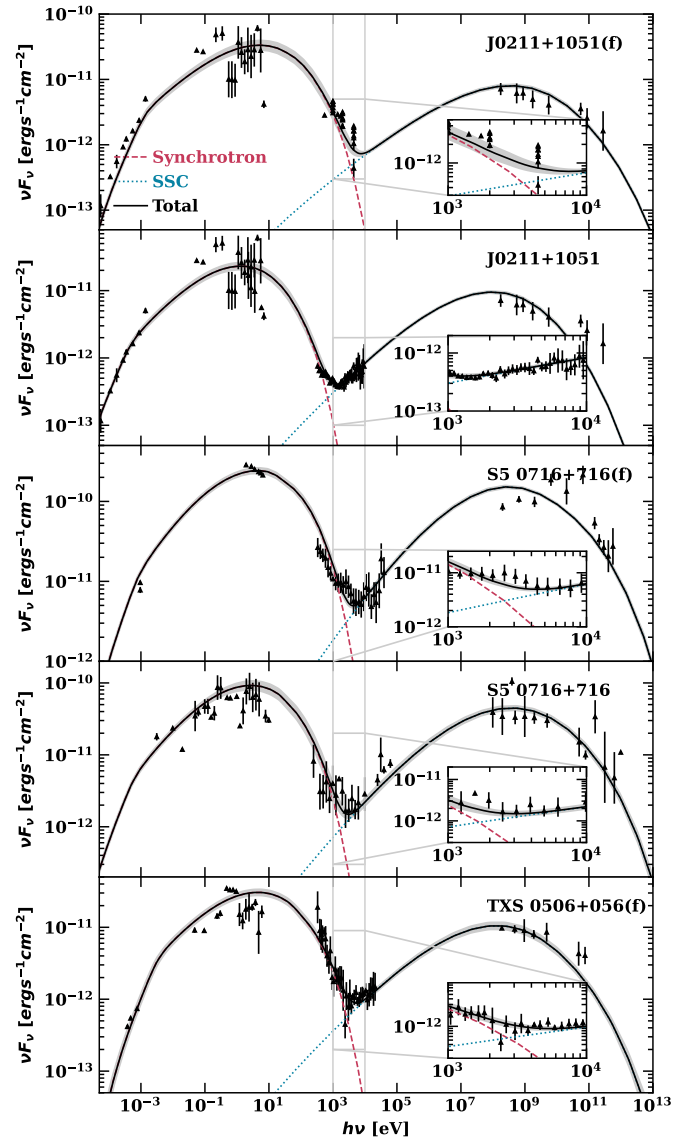
Figure 1. Polarized leptonic jet model fits to all blazars and states. '(f)' denotes a flaring state. Black traces show the expected total SED for the best fit jet parameters. Grey shaded regions around the black trace show 1σ model deviations due to different random magnetic field zones. Vertical grey lines denote *IXPE*'s sensitive band, $1 - 10$ keV, and insets show close-ups of this region.

open source the code to run our model and reproduce the results[2] (Peirson 2022).

Model fit results are shown in Fig. 1. Best fit jet parameters and their respective errors are displayed in Table 2. In Fig. 2 we show the predicted polarization behavior resulting from the jet model fits displayed in Fig. 1. The number of magnetic field zones in the jet

model is selected so that the predicted optical polarization fraction matches the median of the observations (Blinov et al. 2021) as closely as possible. Note that individual realizations of the polarization fraction can vary significantly.

It is useful to compare our polarization predictions to previous studies. Zhang et al. (2019) model TXS 0506+056 using a single zone leptonic emission model with a uniform magnetic field, matching the observed optical polarization degree with a constant polarization dilution factor. They predict an SSC polarization degree of approximately 5% in the X-ray band, rising to 8% at MeV energies. This represents a slightly higher X-ray polariztion fraction, increasing more strongly to high energy. The differences can be attributed to our multizone setup, where multiple magnetic field orientations relative to the line of sight affect the net synchrotron to SSC polarization ratio and its energy dependence (Bonometto & Saggion 1973; Peirson & Romani 2019); multi-zone models generally predict lower SSC polarization degree. We note that our model also propagates synchrotron seed photons between magnetic field zones, further diluting the SSC polarization and increasing sensitivity to the jet geometry.

3. IXPE MEASUREMENT SIMULATIONS

A principal goal of IXPE-ISP source measurements is to detect two different X-ray polarizations – a lower energy, electron synchrotron dominated component and a higher energy component. Assuming an SSC spectrum, we explore whether such a measurement is possible for each of our ISPs with typical IXPE exposures, using IXPE's standard analysis pipeline processing over a 2-8 keV band.

Using ixpeobssim, IXPE's observation simulation software (Pesce-Rollins et al. 2019), we simulate multiple 300 ks and 500 ks observations for each blazar state assuming polarization and flux are fixed to their expected (average) values (i.e. the black traces in Figs. 1, 2). We split the simulated 2-8 keV data into two energy bins: 2-4 keV and 4-8 keV, extracting the polarization fractions by estimating the Stokes' parameters as in Kislat et al. (2015). Figure 3 summarizes the results.

In Fig. 3, energy bins where the true polarization fraction distribution (blue, right-hand-side) is fully below the minimum detectable polarization (MDP$_{99}$) threshold (dotted lines) cannot produce significant ($\gtrsim 3\sigma$) detection of non-zero polarization in the given exposure time. MDP$_{99}$ is the 99th percentile upper confidence bound on polarization fraction for an unpolarized
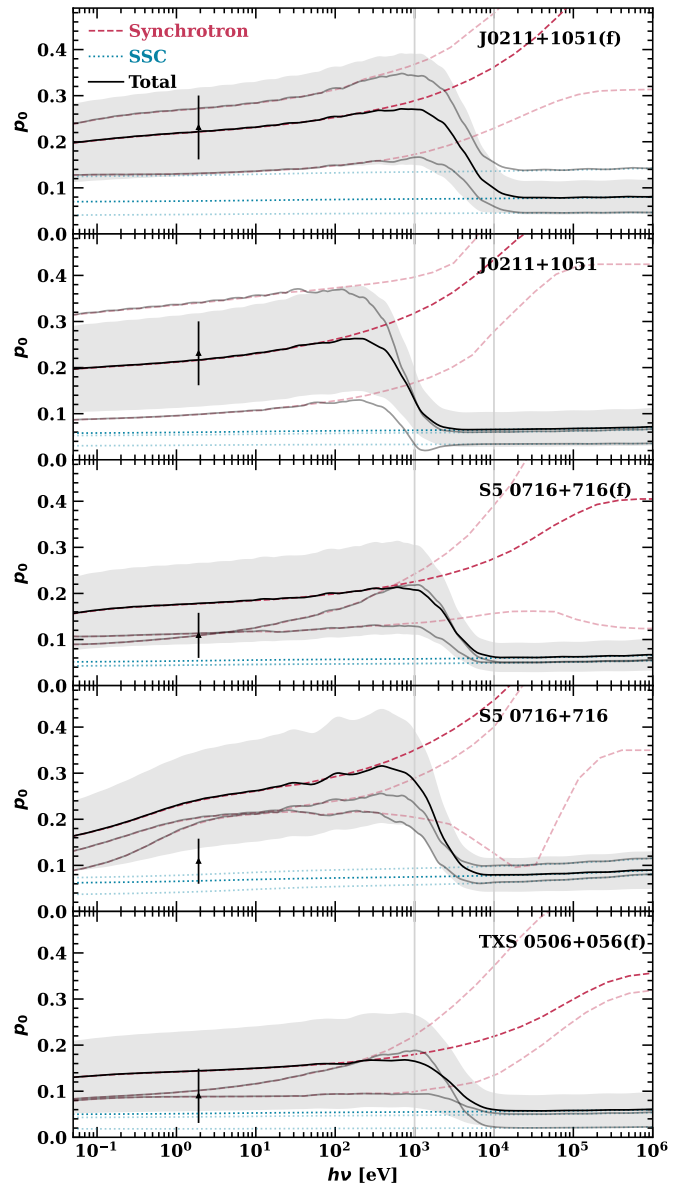
Figure 2. Leptonic (SSC) jet model polarization fraction predictions. The jet models used in each panel are the same as those in Fig. 1. Black observations denote the average measured optical polarization over multiple epochs (MJD 56432 – 57893 for Robopol measured S5 0716+714 and J0211+1051 (Blinov et al. 2021) and MJD 58019 – 58267 for TXS 0506+056). Lines and shaded regions mean the same as Fig. 1 with the addition of two transparent models, which represent randomly selected model realizations.

source. Energy bins with some or all of the true polarization distribution above MDP$_{99}$ can have significant detections, if their actual polarization is in the upper portion of the predicted range – the measurement errors would be approximately given by the measured polarization fraction distributions for the most probable p_0 (red,

Table 2. Polarized jet model best fit parameters. Jet power W_j, electron high energy cutoff before exponential decay E_{max}, electron population power law index α, full conical jet opening angle in lab frame θ_{open}, bulk Lorentz factor Γ_{bulk}, initial magnetic field strength B_0, jet observation angle in lab frame θ_{obs}, and initial equipartition fraction A_{eq}.

Name	$W_j[10^{37}W]$	$E_{max}[10^9 eV]$	α	$\theta_{open}[°]$	Γ_{bulk}	$B_0[10^{-5}T]$	$\theta_{obs}[°]$	A_{eq}
J0211+1051(f)	4.94 ± 0.1	13.4 ± 1.0	2.05 ± 0.01	7.16 ± 0.19	14.8 ± 0.64	5.04 ± 0.2	1.95 ± 0.18	0.81 ± 0.01
J0211+1051	6.48 ± 0.2	9.59 ± 0.1	1.85 ± 0.01	14.1 ± 0.35	7.23 ± 0.15	2.38 ± 0.2	2.31 ± 0.09	0.83 ± 0.02
TXS 0506+056	5.26 ± 0.5	8.03 ± 0.3	1.89 ± 0.01	4.15 ± 0.26	17.3 ± 0.42	9.63 ± 0.3	1.64 ± 0.11	0.98 ± 0.05
S5 0716+714(f)	42.4 ± 5.0	13.4 ± 3.0	1.66 ± 0.02	7.35 ± 0.62	13.2 ± 0.51	2.84 ± 0.6	2.51 ± 0.06	1.05 ± 0.02
S5 0716+714	47.3 ± 11.0	9.49 ± 1.5	1.75 ± 0.09	5.93 ± 0.84	17.0 ± 0.64	3.23 ± 1.5	4.48 ± 0.16	0.84 ± 0.13

NOTE—(f) denotes a flaring state. The number of magnetic field zones N_{zones} is selected from $[1, 7, 19, 37, 64, 128]$. All blazar models shown here use 37 magnetic field zones except CGRaBS J0211+1051, which uses 19.

left-hand-side). Planned observation times for first-year *IXPE* ISP targets, including CGRaBS J0211+1051 and S5 0716+714, are expected to range from 200 ks – 400 ks.

For each blazar and state the two energy bins, 2-4 keV and 4-8 keV, contain different relative synchrotron and SSC contributions. Insets in Fig. 1 give the relative contributions. In non-flaring states, both energy bins are almost entirely dominated by SSC emission so measurement of the synchrotron cutoff component will not be possible.

Low significance polarization fraction measurements, below MDP$_{99}$, are strongly biased away from $p_0 = 0$. Strict non-negativity of p_0 forces measurement posteriors (red, Fig. 3) to be asymmetric and for $\mathbb{E}(\hat{p}_0) > p_0$ (see, esp. CGRaBS J0211+1051 quiescent panel). This highlights the danger of making polarization inferences using low significance point estimates. The measurement bias can be corrected using appropriate p_0 estimators (Simmons & Stewart 1985).

4. DISCUSSION

Under a purely leptonic (SSC) jet model for ISPs, we find that simultaneously detecting significant X-ray polarization from both emission components with a ≤ 500 ks *IXPE* observation is impossible, even considering high p_0 fluctuations (see Fig.3). For the assumptions used here, a 2.5 Ms exposure would be required to measure the median predicted SSC polarization in our brightest source, S5 0716+714, during its high state. Unfortunately, blazar polarization variability may preclude such long observation times. Optical polarization measurements (Blinov et al. 2021) suggest that blazar polarization fraction and PA can vary significantly over time periods < 500 ks. This would result in an incoherent averaging of polarization vectors leading to depolarization. Many blazar models (Marscher 2014) including our own (Fig. 2) predict polarized X-ray electron syn-

chrotron emission to be more variable than the optical (Di Gesu et al. 2022).

If external Compton (EC) contributes significantly to a blazar's high energy emission component, the case for measuring its X-ray polarization becomes even more dim. EC emission is usually assumed to be unpolarized (Zhang & Boettcher 2013) since the external photon field being scattered is assumed incoherent, originating in the broad line region or accretion disk. Even a small EC contribution can make observations more difficult because MDP$_{99} \propto 1/\sqrt{N_{ph}}$. A 10% fractional EC contribution would lower Fig. 3 true polarization fractions by 10% and increase required observation times for the same significance by 23%. Luckily, all three sources considered are classified as BL-Lac objects, typically associated with low EC contributions. Padovani et al. (2019), however, suggest that TXS 0506+056 is an FSRQ in disguise, in which case there might be significant EC contribution to the high energy component.

For the ISPs in flaring states, a significant polarization measurement of the synchrotron cutoff is feasible although still difficult, requiring the blazar to be in a high polarization state. Along the primary synchrotron cutoff we expect an increased expected polarization fraction and variability compared to the optical SED peak (see Fig. 2) as the most Doppler-boosted magnetic field zones increasingly dominate the observed emission (Peirson & Romani 2019). Our model presents the minimal (geometry-induced) increase polarization degree above the primary synchrotron peak; other effects may further increase the dominance of individual zones. For example, in the shock scenario particles are more efficiently accelerated when the magnetic field is aligned along the shock normal (Marscher 2014). Thus chaotic magnetic field zones will vary in their upper electron energy cutoff and that energy can correlate with the global jet geometry. The highest energy electrons contributing X-ray
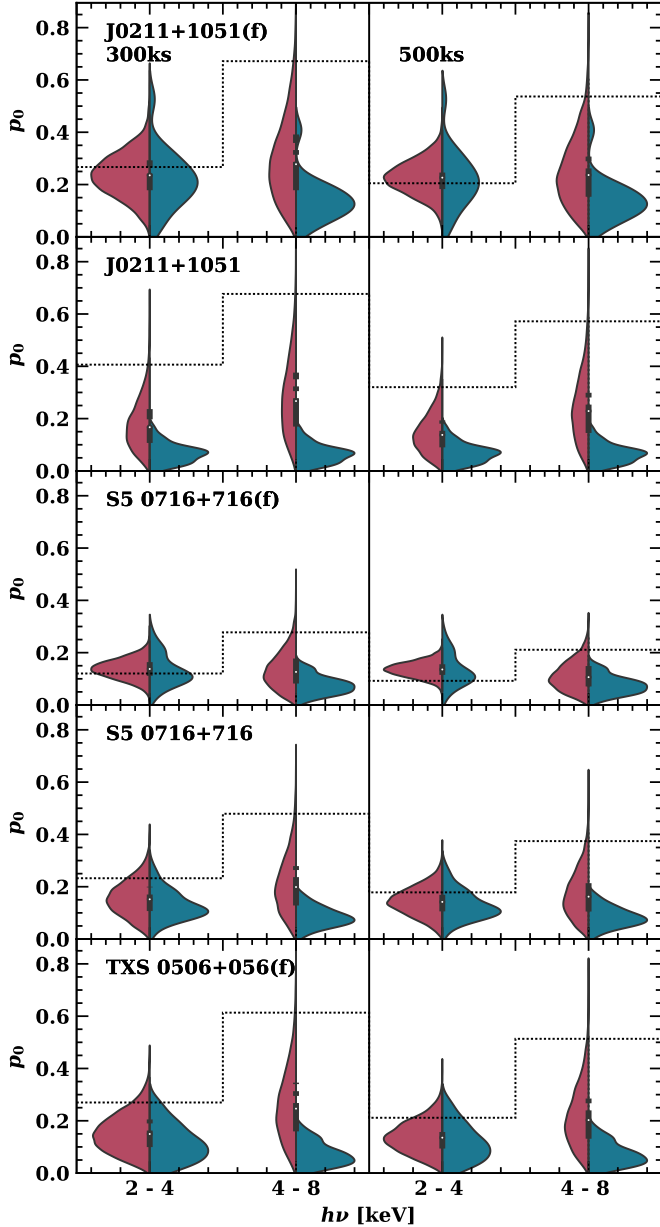
Figure 3. Violin plots of the true polarization fraction distribution (blue, left-hand-side) and the measured polarization fraction distribution (red, right-hand-side) for $2-4\,\mathrm{keV}$ and $4-8\,\mathrm{keV}$ energy bins, and $300\,\mathrm{ks}/500\,\mathrm{ks}$ exposures. The distributions of true polarization fractions are extracted from our jet model fits (Fig. 2) and are the same for both exposure times. Measured polarization fraction distributions assume a single observation with true polarization equal to the expected value. Dashed black traces represent the minimum detectable polarization (MDP$_{99}$) for each measurement bin.

emission are close to the shock, where cooling is limited and the field orientation (and hence polarization) are more highly correlated. Also, Tavecchio et al. (2018) show that immediately downstream of a shock magnetic field compression increases the field perpendicular to the shock normal; this preferential alignment tends to correlate the field orientations and increase net polarization degree, although such correlation decays as turbulence develops downstream. Both these effects may increase polarization at the high energy end of the synchrotron component, improving measurement prospects. In contrast magnetic reconnection scenarios suggest synchrotron cutoff polarization with higher variability but similar net polarization degree to the synchrotron peak emission (Zhang et al. 2020; Tavecchio et al. 2018). Thus comparing X-ray polarization to simultaneous optical polarization degree may be able to distinguish these acceleration scenarios.

Unexpectedly large high energy component polarization arising from non-leptonic jet emission is possible and potentially detectable. Our leptonic (SSC) jet model predicts any high energy component polarization should typically be $0.2-0.35\times$ lower than at the SED optical peak (Peirson & Romani 2019) with the decrement sensitive to the jet geometry. Of course, this ratio is variable and can occasionally fluctuate to large values > 0.5, especially if the peak polarization is low, so only multi-epoch trends or long-term averages have predictive power. In the most optimistic hadronic jet scenario, proton and secondary electron synchrotron dominate the high energy emission component (Zhang & Boettcher 2013; Gao et al. 2019). High energy component X-ray band polarization fractions would be similar to the SED optical peak (Fig. 2), corresponding to a X-ray/optical polarization ratio of 1, extremely unlikely in a SSC dominant leptonic emission model. Although this would provide a much needed polarization fraction boost, a two component detection would remain out of reach, even for a $\leq 500\,\mathrm{ks}$ *IXPE* observation, for all ISPs except S5 0716+714 in its flaring state. Indeed, S5 0716+714 is the first ISP *IXPE* target, planned for a $300\,\mathrm{ks}$ observation on 31st March 2022; a significant polarization detection for both high and low energy components would be a promising indication of non-leptonic jet emission.

If initial *IXPE* observations do not detect significant polarization from either emission component in any ISPs, it will be difficult to rule out non-leptonic processes. Upper polarization fraction limits based on the MDP$_{99}$s in Fig. 3 will be too high to make any useful inference about the polarization ratio of the two emission components, even with a strong synchrotron detection at 2-4 keV. However, the measurements' sensitivity may

be improved. Bayesian neural network analysis of *IXPE* data (Peirson et al. 2021; Peirson & Romani 2021) has been shown to reduce MDP_{99}s by up to 25% compared to the standard *IXPE* analysis pipeline, as well as increasing *IXPE*'s effective energy band to 1-10 keV. We may also tune the energy range of the 'low' and 'high' energy detection windows for an individual source's SED, improving our ability to measure or bound the two components' p_0. Such improved analysis could, for example, make a flaring 4-8 keV S5 0716+714 SSC polarization detection possible with a 500 ks observation – Fig. 3. Although neural network analysis is not yet in production for *IXPE*, a re-analysis of borderline observations could reveal missed discoveries. Looking further ahead, the effective area of future X-ray polarization mission *eXTP* (Zhang et al. 2018) should be four times larger than *IXPE*'s, reducing MDP_{99}s by a factor of 0.5 (Di Gesu et al. 2020). Including both improvements, simultaneous measurement of both ISP emission components with a 500 ks observation is well in scope for all the ISPs considered here.

Facilities: IXPE, NuSTAR, RoboPol, *Swift*, XMM-Newton

Software: ixpeobbsim, SSCpol

REFERENCES

Abdo, A. A., Ackermann, M., Agudo, I., et al. 2010, ApJ, 716, 30, doi: 10.1088/0004-637X/716/1/30

Blandford, R., Meier, D., & Readhead, A. 2019, ARA&A, 57, 467, doi: 10.1146/annurev-astro-081817-051948

Blinov, D., Kiehlmann, S., Pavlidou, V., et al. 2021, MNRAS, 501, 3715, doi: 10.1093/mnras/staa3777

Bonometto, S., & Saggion, A. 1973, Astronomy and Astrophysics, 23, 9. http://adsabs.harvard.edu/abs/1973A%26A....23....9B

Di Gesu, L., Ferrazzoli, R., Donnarumma, I., et al. 2020, Astronomy and Astrophysics, 643, A52, doi: 10.1051/0004-6361/202037886

Di Gesu, L., Tavecchio, F., Donnarumma, I., et al. 2022, Testing particle acceleration models for BL LAC jets with the Imaging X-ray Polarimetry Explorer, Tech. rep. https://ui.adsabs.harvard.edu/abs/2022arXiv220109597D

Gao, S., Fedynitch, A., Winter, W., & Pohl, M. 2019, Nature Astronomy, 3, 88, doi: 10.1038/s41550-018-0610-1

Hovatta, T., Lindfors, E., Kiehlmann, S., et al. 2021, A&A, 650, A83, doi: 10.1051/0004-6361/202039481

IceCube Collaboration, Aartsen, M. G., Ackermann, M., et al. 2018, Science, 361, eaat1378, doi: 10.1126/science.aat1378

Kislat, F., Clark, B., Beilicke, M., & Krawczynski, H. 2015, Astroparticle Physics, 68, 45, doi: 10.1016/j.astropartphys.2015.02.007

Kochenderfer, M. J., & Wheeler, T. A. 2019, Algorithms for Optimization (Cambridge, MA, USA: MIT Press)

Liodakis, I., Peirson, A. L., & Romani, R. W. 2019, ApJ, 880, 29, doi: 10.3847/1538-4357/ab2719

Liodakis, I., Romani, R. W., Filippenko, A. V., et al. 2018, MNRAS, 480, 5517, doi: 10.1093/mnras/sty2264

Marscher, A. P. 2014, ApJ, 780, 87, doi: 10.1088/0004-637X/780/1/87

Padovani, P., Oikonomou, F., Petropoulou, M., Giommi, P., & Resconi, E. 2019, Monthly Notices of the Royal Astronomical Society: Letters, 484, L104, doi: 10.1093/mnrasl/slz011

Peirson, A. 2022, alpv95/SSCpol: v1.3.1, Zenodo, doi: 10.5281/zenodo.6450411

Peirson, A. L., & Romani, R. W. 2018, ApJ, 864, 140, doi: 10.3847/1538-4357/aad69d

—. 2019, ApJ, 885, 76, doi: 10.3847/1538-4357/ab46b1

Peirson, A. L., & Romani, R. W. 2021, arXiv:2107.08289 [astro-ph]. http://arxiv.org/abs/2107.08289

Peirson, A. L., Romani, R. W., Marshall, H. L., Steiner,
    J. F., & Baldini, L. 2021, Nuclear Instruments and
    Methods in Physics Research Section A: Accelerators,
    Spectrometers, Detectors and Associated Equipment,
    986, 164740, doi: 10.1016/j.nima.2020.164740

Pesce-Rollins, M., Lalla, N. D., Omodei, N., & Baldini, L.
    2019, Nuclear Instruments and Methods in Physics
    Research A, 936, 224, doi: 10.1016/j.nima.2018.10.041

Potter, W. J., & Cotter, G. 2012, Monthly Notices of the
    Royal Astronomical Society, 423, 756,
    doi: 10.1111/j.1365-2966.2012.20918.x

Rubinstein, R. Y., & Kroese, D. P. 2004, The Cross
    Entropy Method: A Unified Approach To Combinatorial
    Optimization, Monte-carlo Simulation (Information
    Science and Statistics) (Berlin, Heidelberg:
    Springer-Verlag)

Simmons, J. F. L., & Stewart, B. G. 1985, Astronomy and
    Astrophysics, 142, 100. https://ui.adsabs.harvard.edu/
    abs/1985A&A...142..100S/abstract

Tavecchio, F., Landoni, M., Sironi, L., & Coppi, P. 2018,
    MNRAS, 480, 2872, doi: 10.1093/mnras/sty1491

Weisskopf, M. C., Soffitta, P., Baldini, L., et al. 2021, arXiv
    e-prints, arXiv:2112.01269.
    https://arxiv.org/abs/2112.01269

Wierzcholska, A., & Siejkowski, H. 2016, MNRAS, 458,
    2350, doi: 10.1093/mnras/stw425

Zhang, H., & Boettcher, M. 2013, The Astrophysical
    Journal, 774, 18, doi: 10.1088/0004-637X/774/1/18

Zhang, H., Fang, K., Li, H., et al. 2019, The Astrophysical
    Journal, 876, 109, doi: 10.3847/1538-4357/ab158d

Zhang, H., Li, X., Giannios, D., et al. 2020, The
    Astrophysical Journal, 901, 149,
    doi: 10.3847/1538-4357/abb1b0

Zhang, S., Santangelo, A., Feroci, M., et al. 2018, The
    enhanced X-ray Timing and Polarimetry mission - eXTP,
    Vol. 62, doi: 10.1007/s11433-018-9309-2